A Tropical Count of Real Bitangents to Plane Quartic Curves

Alheydis Geiger Marta Panizzut

Max-Planck-Institute for Mathematics in the Sciences,
Leipzig, Germany

{alheydis.geiger,marta.panizzut}@mis.mpg.de

Submitted: Mar 11, 2022; Accepted: May 13, 2023; Published: Jun 30, 2023

Abstract

A smooth tropical plane quartic curve has seven tropical bitangent classes. Their shapes can vary within the same combinatorial type of curve. We study deformations of these shapes and we show that the conditions determined by Cueto and Markwig for lifting them to real bitangent lines are independent of the deformations. From this we deduce a tropical proof of Plücker and Zeuthen's count of the number of real bitangents to smooth plane quartic curves.

Mathematics Subject Classifications: 14T15, 14T20

1 Introduction

The number of bitangent lines to a smooth plane quartic curve is a classical result from the 19th century. Plücker proved in 1834 that such a curve in the complex projective plane has 28 bitangents [19]. Building on an extensive first count by Plücker [20], Zeuthen proved that a smooth quartic curve can have either 4, 8, 16 or 28 real bitangents depending on the topology of the underlying real curve in the real projective plane [21]. In this paper we provide a count of real bitangents to a tropically smooth plane algebraic quartic curve using computations and techniques from tropical geometry.

Smooth tropical quartic curves can have exactly 7 or infinitely many bitangent tropical lines grouped into 7 equivalence classes modulo continuous translations that preserve bitangency. This was proven by Baker et al. [2] using the theory of divisors on tropical curves. Bitangents to non-smooth tropical quartics were investigated in [13].

Questions about lifting tropical bitangents were first considered by Chan and Jiradilok [5] for K_4-curves. Len and Markwig [14] showed that under certain genericity conditions, each class lifts to four bitangent lines over the complex Puiseux series, reproducing Plücker's theorem for tropically smooth quartic curves. These four lifts can be realized

by more than one representative in the class and with different multiplicities. Cueto and Markwig [6] proved that each class lifts either zero or four times to real bitangent lines, and they remarked that these real lifts are always totally real, meaning that also the tangency points have real coordinates. As a consequence, every number of real bitangents appearing for a tropically smooth real quartic curve must be divisible by 4. However, a tropical proof of why only the numbers 4, 8, 16 and 28 are observed was still open. The main result of this paper bridges this gap by providing a tropical version of Plücker and Zeuthen's count.

Theorem 1. *Let* Γ *be a generic tropicalization of a smooth quartic plane curve defined over a real closed complete non-Archimedean valued field. Either* 1*,* 2*,* 4 *or* 7 *of its bitangent classes admit a lift to real bitangents near the tropical limit. Every smooth quartic curve whose tropicalization is generic has either* 4*,* 8*,* 16 *or* 28 *totally real bitangents.*

To prove this theorem, we relied on the classification of the combinatorial structure of the bitangent classes by Cueto and Markwig [6]. Smooth tropical quartics are dual to unimodular triangulations of the fourth dilation of the standard 2-simplex. The dual subdivision is also called the combinatorial type of a quartic. The shapes of bitangent classes of tropical quartic curves with the same combinatorial type do not need to be equal, as illustrated in Example 3. This motivates the introduction of deformation classes, which collect for each bitangent class the varying shapes that appear within the same combinatorial type. We provide a classification of deformation classes of tropical bitangents that uniquely depend on the combinatorics of the tropical curve.

Theorem 2. *There are* 24 *deformation classes of tropical bitangent classes to generic smooth tropical quartic curves modulo* S_3*-symmetry. Orbit representatives of their dual deformation motifs are summarized in Figure 11.*

The real lifting conditions, i.e., the conditions for admitting a lift to a bitangent over a real closed field with a non-Archimedean valuation, determined by Cueto and Markwig [6], provide us with local information on the number of lifts of each bitangent shape.

The cones in the secondary fan of $4\Delta_2$ that induce unimodular triangulations parameterize tropically smooth plane quartics. Bitangent shapes can vary within a given cone, since they depend on the edge lengths of the tropical quartic curve, rather then solely on the input triangulation. However, Theorem 14 states that the lifting conditions over a real closed complete non-Archimedean valued field depend solely on the triangulations. This motivates the construction of deformation classes of bitangent shapes, which are determined by the given triangulation and provide explicit sign rules for lifting each deformation class (see Table 5).

Using `polymake` [8], we enumerate the deformation classes for every combinatorial type of tropical quartic curves. We then check the real lifting conditions obtaining the expected number of real bitangent lines. We impose the same genericity assumptions as in [6, 14] and we discuss them further in Section 2. In particular, they include the smoothness of the tropicalized curve. Note that the count over the reals follows from working over a real closed field by Tarski-Seidenberg's Transfer Principle [3, Theorem

1.4.2]. Real tropicalization goes back to work of Maslov [17] and the study of logarithmic limit sets of (real) algebraic varieties, see also [1].

This paper is organized as follows. In Section 2, we introduce the main definitions and we report the classification of tropical bitangent classes and their lifting conditions, as introduced in [6]. We assume that the reader is familiar with basic definitions and results on tropical curves and regular triangulations. We refer to [7, 15] for further details. Deformation classes are defined and classified in Section 3. In Section 4, we study their real lifts and prove Theorem 1. The proof is based on the enumeration of deformation classes in `polymake`. The technical description of the algorithms and their implementation can be found in [10]. The proofs for the classification are always constructed by providing details of few cases, and then summarizing the main ideas of the remaining ones. More examples and figures are collected in the Appendix A in order to provide further geometric intuition for the definitions and proofs.

2 Tropical quartic curves and their bitangents

A plane quartic curve $V(f)$ is the zero set of a polynomial of degree four

$$\begin{aligned} f(x,y) = a_{00} + a_{10}x + a_{01}y + a_{20}x^2 + a_{11}xy + a_{02}y^2 + a_{30}x^3 + a_{21}x^2y \\ + a_{12}xy^2 + a_{03}y^3 + a_{40}x^4 + a_{31}x^3y + a_{22}x^2y^2 + a_{13}xy^3 + a_{04}y^4. \end{aligned} \tag{1}$$

We consider the tropicalization of curves defined over a real closed complete non-archimedean valued field $\mathbb{K}_{\mathbb{R}}$ and its algebraic closure $\mathbb{K}$. For the tropicalization of curves, we use the *max*-convention. We write λ_{ij} for the valuations of the coefficients of the polynomial, i.e., $\lambda_{ij} = \mathrm{val}(a_{ij})$. Then, $\mathrm{Trop}(V(f))$ is the tropical curve define by the tropical polynomial with coefficients $-\lambda_{ij}$.

We assume that the Newton polygon of f is the fourth dilation of the standard 2-dimensional simplex $4\Delta_2$. The polygon $4\Delta_2$ contains 15 lattice points p_{ij} corresponding to the monomials $x^i y^j$ of f. By duality, the combinatorics of the tropical curve $\Gamma = \mathrm{Trop}(V(f))$ is determined by the subdivision $\mathcal{T}$ (of the lattice points) of $4\Delta_2$ induced by the coefficients $-\lambda_{ij}$. We use the notation $\cdot^\vee$ to refer to the dual of a vertex or an edge of Γ in $\mathcal{T}$, and viceversa. We only consider smooth tropical plane quartic curves, so the subdivisions of $4\Delta_2$ are unimodular triangulations. In particular, all lattice points in $4\Delta_2$ are vertices in the triangulation $\mathcal{T}$. The set of points in $\mathbb{R}^{15}$ inducing the same subdivision is a relative open cone called the *secondary cone* and denoted $\Sigma(\mathcal{T})$. For a point $c \in \Sigma(\mathcal{T})$, we use the notation Γ_c to indicate the tropical quartic curve defined by the tropical polynomial with coefficients given by the coordinates of c.

Regular unimodular triangulations of $4\Delta_2$ have been enumerated by Brodsky et al. in [4]. They counted 1278 orbits of combinatorial types under the action of the symmetric group S_3. This group acts on the homogenization of the lattice points of $4\Delta_2$ and on the corresponding monomials of the polynomial f and its tropicalization $\mathrm{Trop}(f)$.

A tropical line Λ is *bitangent* to a smooth tropical plane quartic curve Γ if their intersection $\Lambda \cap \Gamma$ has two components with stable multiplicity 2, or one component with

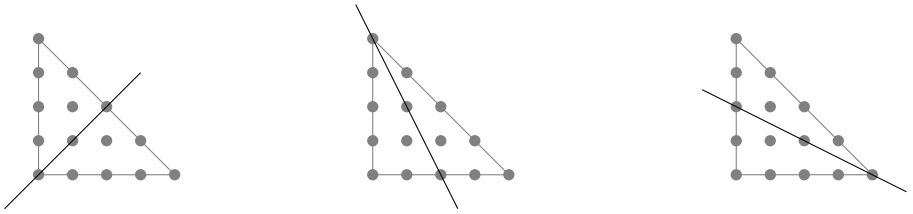

Figure 1: Actions of the transpositions in S_3 on $4\Delta_2$.

stable multiplicity 4. See [15, Section 3.6] for an introduction to stable intersections. We always assume that tropical bitangent lines are non-degenerate, i.e., each tropical line consists of a vertex and three adjacent rays with directions $-e_1$, $-e_2$ and $e_1 + e_2$ given by the standard basis of $\mathbb{R}^2$. For an impression of tropical bitangent lines, see Figure 3.

A tropical quartic curve Γ has exactly 7 or infinitely many tropical bitangents. The collection of bitangents can be grouped into 7 equivalence classes modulo continuous translations that preserve bitangency as shown in [2]. Formally, the *tropical bitangent classes* of a tropical quartic Γ are defined as the connected components of $\mathbb{R}^2$ containing the vertices of tropical bitangents in the same equivalence class. Up to S_3-symmetries, they refine into 41 *shapes of tropical bitangent classes* given by coloring the points in the class belonging to Γ, see Figure 2. Since a non-degenerate tropical line is determined by its vertex, bitangent classes formally live in the dual plane. They are connected polyhedral complexes, which are also min-tropical convex sets [6, Theorem 1.1, Corollary 3.3]. To improve the visualization, we draw the curve and its bitangent classes on the same plane.

As remarked by Cueto and Markwig [6], the shapes of tropical bitangent classes of a smooth tropical quartic curve Γ impose combinatorial constraints on the regular unimodular triangulation of $4\,\Delta_2$ dual to Γ. More precisely, the existence of a representative of a certain shape determines specific subcomplexes that must be contained in the triangulation, see Figure 4. Such a subcomplex is only a necessary condition for the presence of its corresponding tropical bitangent shape. Given a smooth tropical quartic curve Γ, the shapes of its bitangent classes are not fully determined by the combinatorial type of Γ, but they also depend on the length of the edges, as the following example illustrates. This motivates us to introduce deformation classes of tropical bitangents in the following section.

Example 3. We consider the quartic curve dual to the triangulation $\mathcal{T}$ in Figure 3a. The colored subcomplex of $\mathcal{T}$ corresponds to shapes (E), (F) and (J) in the classification in Figure 2. Let $\mathbf{a}$ denote the coefficient vector of an algebraic curve of degree 4 with entries ordered as in (1).

We remark that there exists an equivalence class of bitangents of Γ which adopts different shapes for different choices of $\lambda = \mathrm{val}(\mathbf{a}) \in \Sigma(\mathcal{T})$. We observe shape (E) when choosing $\lambda_1 = (0{,}5{,}5{,}9{,}8{,}5{,}6.5{,}9{,}9{,}4{,}2{,}7{,}8{,}7{,}1)$, see Figure 3b. For $\lambda_2 = (0{,}5{,}5{,}9{,}8{,}5{,}6{,}9{,}9{,}4{,}2{,}7{,}8{,}7{,}1)$ we obtain shape (J) as in Figure 3c. Figure 3d shows shape (F), which appears for $\lambda_3 = (0{,}5{,}5{,}9{,}8{,}5{,}5.5{,}9{,}9{,}4{,}1{,}7{,}8{,}7{,}1)$.

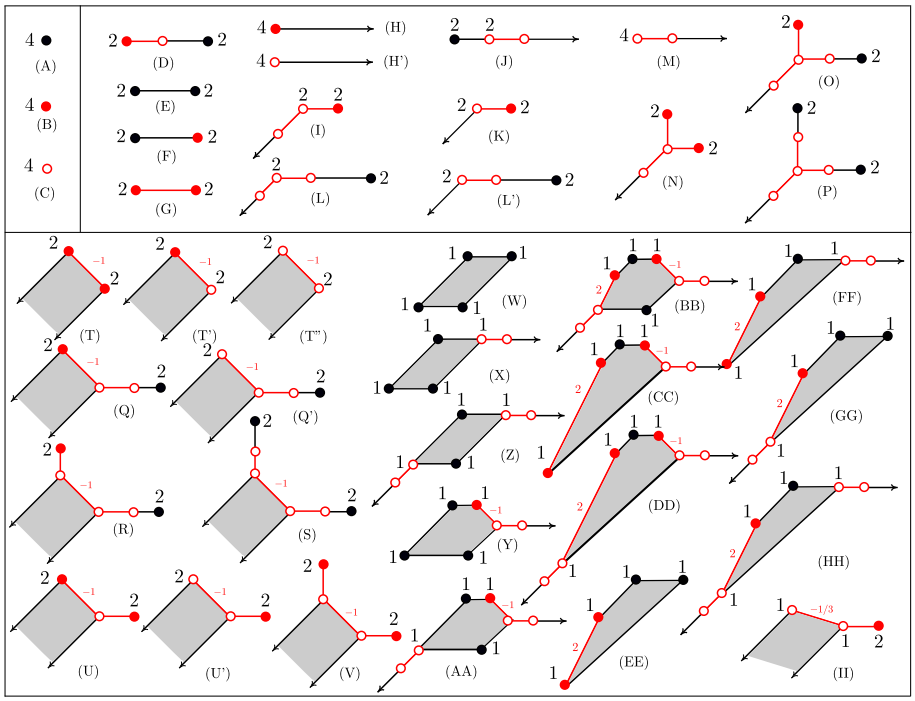

Figure 2: Shapes of bitangent classes on smooth quartics up to S_3-symmetry. The black numbers above the vertices indicate the lifting representatives in each class and their lifting multiplicities. Red vertices or line segments are contained in the quartic curve, a red vertex filled with white coincides with a vertex of the quartic curve. Figure taken from [6, Figure 6].

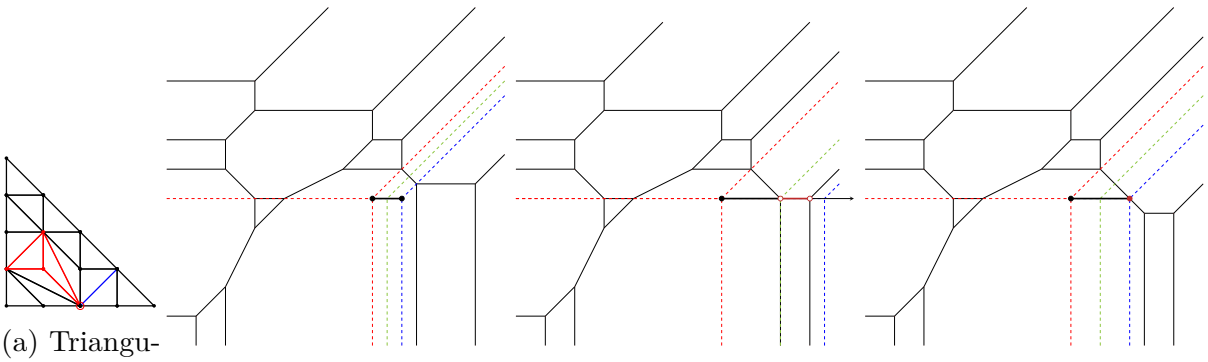

(a) Triangulation $\mathcal{T}$ (b) Shape (E) (c) Shape (J) (d) Shape (F)

Figure 3: The dual triangulation does not fix the shapes of the bitangent classes, since they can change when choosing different edge lengths for the curve.

Let Γ be a smooth tropical quartic curve and $V(f)$ a smooth plane quartic curve defined over $\mathbb{K}$ such that $\mathrm{Trop}(V(f)) = \Gamma$. Following [14, Definition 2.8], we say that a tropical bitangent Λ with tangency points P and P' lifts over $\mathbb{K}$ if there exists a bitangent ℓ to $V(f)$ defined over $\mathbb{K}$ with tangency points p and p' such that

$$\mathrm{Trop}(V(f)) = \Gamma, \quad \mathrm{Trop}(\ell) = \Lambda, \quad \mathrm{Trop}(p) = P, \quad \text{and} \quad \mathrm{Trop}(p') = P'.$$

The number of such ℓ's is the *lifting multiplicity* of Λ. In an equivalence class, the number of tropical bitangents which lift and their lifting multiplicities can be one, two or four, see [14, Theorem 4.1].

Similarly, we are interested in the number of *real* lifts, that is, the lifting multiplicity when $V(f)$ and ℓ are defined over $\mathbb{K}_{\mathbb{R}}$. In this case, as shown by Cueto and Markwig [6], every bitangent class of a given shape has either zero or four lifts to real bitangents. Moreover, the existence of a lift uniquely depends on the signs s_{ij} of the coefficients a_{ij} of the polynomial f. Table 3 in Section 4 summarizes these conditions.

Lifting problems were studied under the genericity constraints explained in [6, Remark 2.10], which also apply in our results next to the assumptions that the tropical curve Γ is smooth and that the tropical bitangent lines are non-degenerate. The assumption that if the tropical curve Γ contains a vertex adjacent to three bounded edges with directions $-e_1$, $-e_2$ and $e_1 + e_2$, the shortest of these edges is unique will be particularly relevant in our analysis of the lifting conditions of shape (C).

We conclude this section by fixing some notation and conventions. We follow the labeling of shapes of bitangent classes and the color patterns introduced in [6] by Cueto and Marking, see Figures 2 and 4. The group S_3 acts on bitangent shapes and their dual subcomplexes. We refer to the bitangent shapes and subcomplexes in Figures 2 and 4 as in *identity position*. We indicate the different elements in the orbit of a bitangent shape not in identity position by adding the element of S_3 acting on it to the index of the shape. For example, the notation $(\mathrm{B})_{(xy)}$ means that the bitangent class has shape (B) with dual complex given by the action of $(x\,y)$ on the complex in identity position.

3 Deformation classes of tropical bitangents

In this section we introduce deformation classes of tropical bitangents and we classify them. Our terminology is inspired by the one introduced in [11, 18] for the classification of the combinatorial positions of tropical lines on cubic surfaces.

Definition 4. Let Γ be a tropical smooth quartic curve with dual triangulation $\mathcal{T}$, and let B be a bitangent class of Γ of a fixed shape. The *dual bitangent motif* of (Γ, B) is the subcomplex of $\mathcal{T}$ that is fully and uniquely determined by the shape of B and its position with respect to Γ. Dual bitangent motifs are classified in [6, Figure 19].

In pictures of dual bitangent motifs, we use the same color coding as Cueto and Markwig [6]. Black and colored solid edges must be part of the triangulations, while dotted ones represent possible edges, of which one must occur. Black vertices are always present,

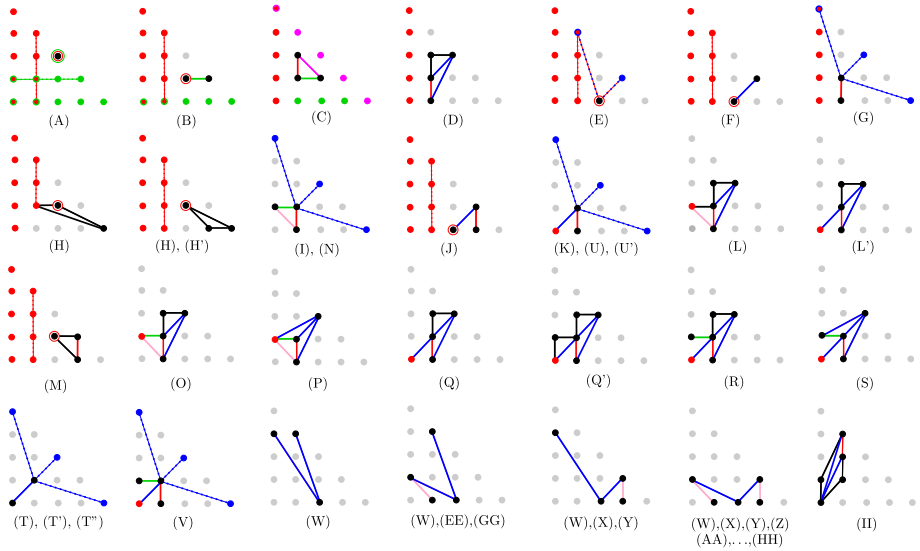

Figure 4: Dual bitangent motifs of bitangent classes. The color coding is explained in [6, Remark 4.13]. Figure taken from [6, Figure 19].

while the colored ones are endpoints of colored possible edges or they form a triangle with an edge of the same color. Different colors correspond to different types of tangencies, see [6, Remark 4.13].

The summary of the dual bitangent motifs as shown in Figure 4 is very condensed, and, as a consequence, for some figures with dotted edges not all combinations lead to the assigned bitangent shape. For example, when choosing the red and green edges $\overline{p_{10}p_{11}}$ and $\overline{p_{01}p_{11}}$ in the picture of (A), the shape, which will occur, will be either (S) or (P), but never (A). Therefore, the dual bitangent motifs will be subdivided more in the following classification of the deformation classes.

Definition 5. Given a tropical quartic Γ_c with dual triangulation $\mathcal{T}$, $c \in \Sigma(\mathcal{T})$, and a tropical bitangent class B, we say that a tropical bitangent class B' is in the same *deformation class* as B if the following conditions are satisfied:

- ▷ There exists $\Gamma_{c'}$ with $c' \in \Sigma(\mathcal{T})$ having B' as one of its bitangent classes.
- ▷ There is a continuous deformation from Γ_c to $\Gamma_{c'}$ given by a path in the secondary cone $\Sigma(\mathcal{T})$ from c to c' that induces B to change to B'.

We use the notation B_ω to indicate the deformation of B in Γ_ω for ω in the path. Given a unimodular triangulation $\mathcal{T}$ of $4\Delta_2$ and a dual quartic curve Γ, let $\mathcal{D}$ be the deformation class of one of its seven bitangent classes. The *dual deformation motif of* $(\mathcal{T},\mathcal{D})$ is the union of the dual bitangent motifs of all shapes belonging to bitangent classes in $\mathcal{D}$.

We label deformation classes using the letters of the shapes of tropical bitangents. In Example 3 we saw a deformation class (E J F). If the class contains the image of shapes under the action of an element $\sigma \in S_3$, we use the notation $+\sigma$. We remark that σ acts on

all shapes in the deformation class, but some of them might be invariant. For example, the deformation class (B H' H)+(yz) consists of the shapes (B), (H'), (H) = $(\text{H})_{(yz)}$, $(\text{H}')_{(yz)}$ and $(\text{B})_{(yz)}$.

Remark 6. Each smooth tropical quartic Γ has 7 deformation classes, and it follows from the definition that they only depend on the dual triangulation $\mathcal{T}$ of Γ. Changing the coefficients defining Γ in the secondary cone $\Sigma(\mathcal{T})$ induces a variation in the shapes of the tropical bitangents within the deformation class.

In order to classify deformation classes, we need to distinguish between the different subcomplexes which give a bitangent shape, e.g. the two different choices of blue edges for shape (E). We have to do this because the combinatorial type of the curve determines how the shapes can deform.

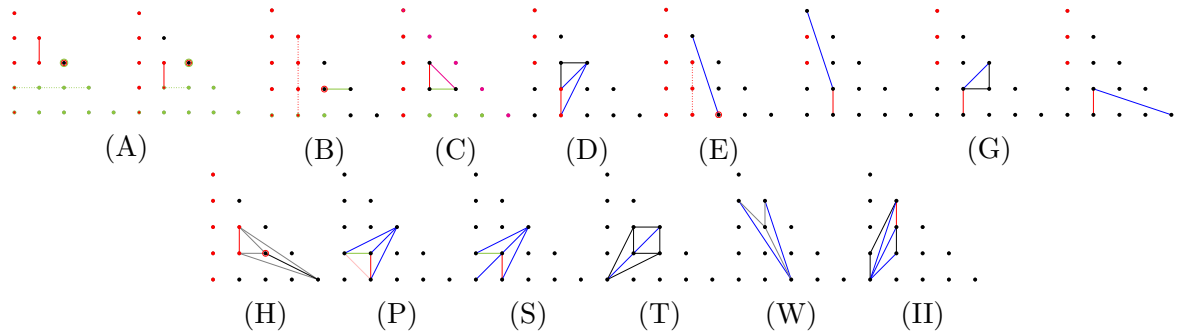

Figure 5: Dual bitangent motifs of bitangent classes with constant shape in their deformation class.

Lemma 7. *Let Γ be a tropical smooth quartic curve dual to a triangulation $\mathcal{T}$ of $4\Delta_2$. Let B be a bitangent class of Γ with dual bitangent motif belonging to the collection in Figure 5, modulo S_3-symmetry. Then, the shape of the bitangent classes is constant in the deformation class of B.*

Proof. The proof works similarly for each of the cases. The main argument for each case is that due to the combinatorial structure of $\mathcal{T}$, the two tangencies cannot change the type of their intersection, and this fully determines the bitangent class and its shape. We explain the details for shape (E) and summarize the remaining cases in Table 1.

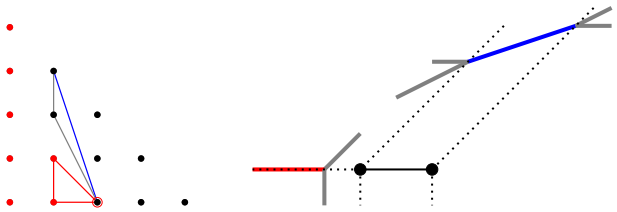

Figure 6: Example of a dual bitangent motif with constant shape (E).

Let B be a bitangent class of shape (E). We may assume that the dual bitangent motif looks as in Figure 6. One tangency point is a transversal intersection in the edge of Γ

dual to $E = \overline{p_{20}p_{13}}$. The second tangency point is a non-transversal intersection of the horizontal ray of Λ with the bounded edge of Γ dual to $\overline{p_{10}p_{11}}$ or $\overline{p_{11}p_{12}}$. We can exclude the edge $\overline{p_{12}p_{13}}$ since it does not define a dual bitangent motif of shape (E).

The bitangent class B is a line segment. Its two endpoints are determined by intersecting rays with direction $-(e_1 + e_2)$ through the vertices of the edge $E^\vee$ of Γ with a ray with direction e_1 passing through the non-transversal intersection. See Figure 6 for an example. Independently of the lengths of the edges of Γ, the endpoints of B cannot lie in Γ because of the slopes of the edges of Γ that connect the vertices $\Delta(p_{10}p_{11}p_{20})^\vee$ and $\Delta(p_{12}p_{13}p_{20})^\vee$.

Table 1 contains the remaining bitangent classes from the statement. For each deformation class, we draw the dual deformation motif in the dual triangulation and the relevant part of the tropical quartic curve. When there are several possible dual bitangent motifs condensed in a picture, we draw one tropical curve dual to only one of them. From the combinatorial shape of the tropical curve, we can see that changes of edge lengths cannot induce a deformation of the shape of the bitangent class. □

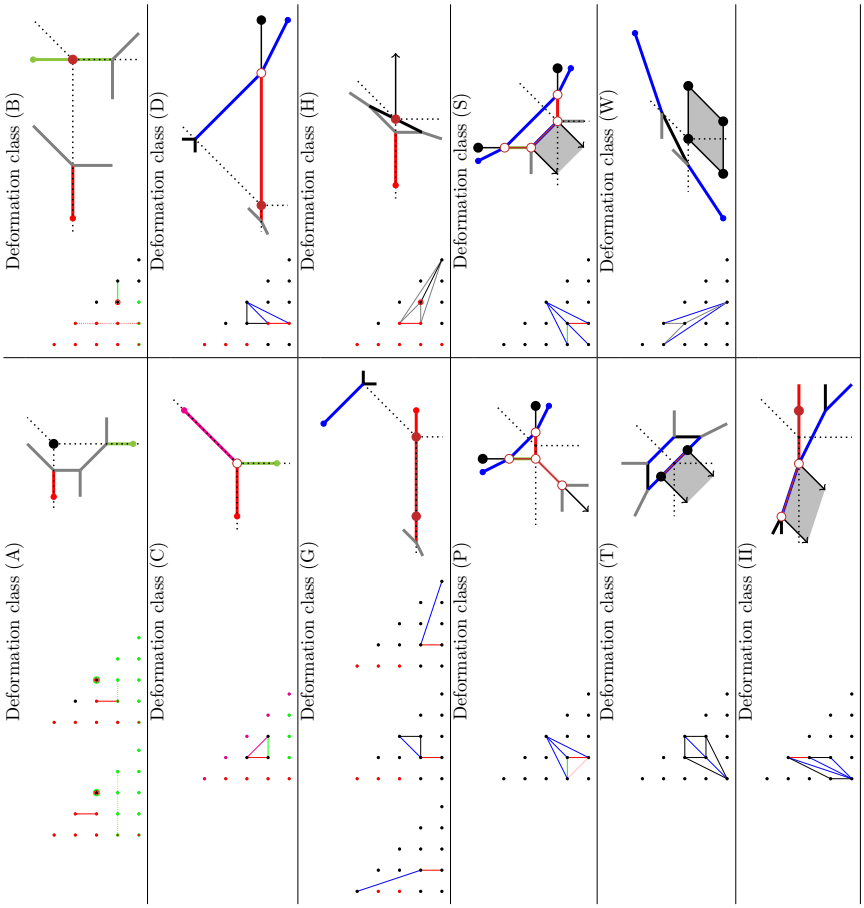

Table 1: Deformation classes from Lemma 7. A thickened vertex of an edge in the curve indicates that this edge must be bounded.

Lemma 7 describes the deformation classes containing bitangent classes of a unique

shape. We now consider two cases of deformation classes of not constant shape. Further details on the proofs of the upcoming lemmas can be found in [9].

Lemma 8. *Let Γ be a tropical smooth plane quartic curve with dual triangulation $\mathcal{T}$ and B a bitangent class with dual bitangent motif contained in one of the subcomplexes depicted in Figure 7 modulo S_3-symmetry. For every $c \in \Sigma(\mathcal{T})$, the bitangent class B_c has shapes (E), (F) or (J).*

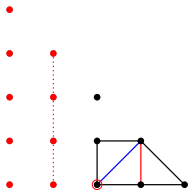

Figure 7: Dual deformation motifs of deformation class (E J F).

Proof. Let B be a bitangent class with dual bitangent motif as in Figure 7. The first tangency point is the transversal intersection of the diagonal ray of the bitangent with the edge of Γ dual to $E = \overline{p_{20}p_{31}}$. The second tangency point is a non-transversal intersection with one of the three bounded edges of Γ dual to $\overline{p_{10}p_{11}}$, $\overline{p_{11}p_{12}}$ or $\overline{p_{12}p_{13}}$. Since $\mathcal{T}$ is unimodular, we remark that the subcomplexes we are considering contain the dual bitangent motifs of shapes (E), (F) and (J) in identity position. We need to show that for any Γ_c with $c \in \Sigma(\mathcal{T})$ the bitangent class B can only deform between these shapes.

Let E' be the vertical red dotted edge in $\mathcal{T}$ that forms a triangle with the red circled lattice point p_{20}. The bounded edge of Γ dual to E' will always have y-coordinate smaller than the vertex $v = \Delta(p_{20}p_{31}p_{21})^\vee$. Hence, for any Γ_c the tangent points of the bitangent class are contained in the edge dual to E and the bounded edge dual to E'.

Changes in the length of the edge dual to E influence the position of the intersections. Depending on the y-coordinate of the bounded edge dual to E' in comparison with the vertex v, we obtain shape (E), (J) or (F) for B. This is illustrated in Figure 8 for the case $E' = \overline{p_{12}p_{13}}$. The other two cases are analogous. We cannot obtain another shape for B because the value of the x-coordinate of the points in the edge dual to E' and of v do not influence the shape. □

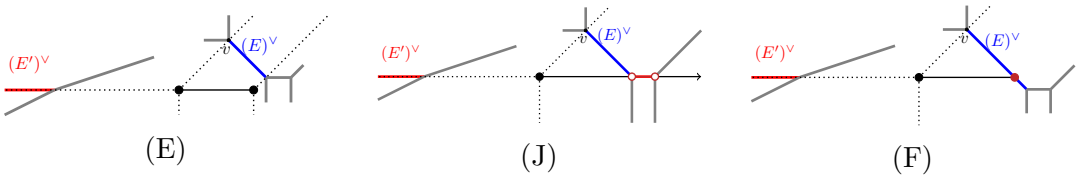

Figure 8: Deformation of bitangent shapes (E), (J) and (F).

Lemma 9. *Let Γ be a tropical smooth plane quartic curve dual to a triangulation $\mathcal{T}$. Let B be a bitangent class with dual bitangent motif contained in one of the two cases illustrated in Figure 9, modulo S_3-symmetry. For every $c \in \mathcal{T}$, the bitangent class B_c can deform through the shapes (G), (K), (U), (U'), (T), (T'), (T"), (V) and into the images of the action by $(x\,y)$ of the shapes (T'), (U), (U'), (K) and (G).*

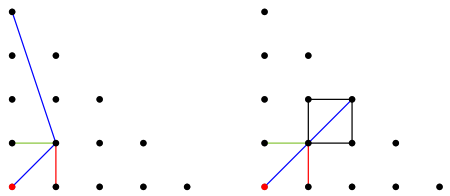

Figure 9: The two dual deformation motifs of deformation class (G K U U' T T' T" V)+$(x\,y)$.

Proof. We distinguish the two cases in Figure 9 depending on whether the edge $\overline{p_{11}p_{22}}$ or the edge $\overline{p_{11}p_{04}}$ is contained in the triangulation $\mathcal{T}$. Figure 10 shows deformations of B into the claimed shapes by edge length changes of Γ when the blue edge is $E = \overline{p_{11}p_{22}}$. Analogous pictures can be drawn for $\overline{p_{11}p_{04}}$. The edge lengths can be interpreted in terms of relative positions of vertices of Γ. This approach is considered in the proof of the classification of bitangent shapes in [6, Section 4]. It remains to argue that these are the only shapes B can deform into.

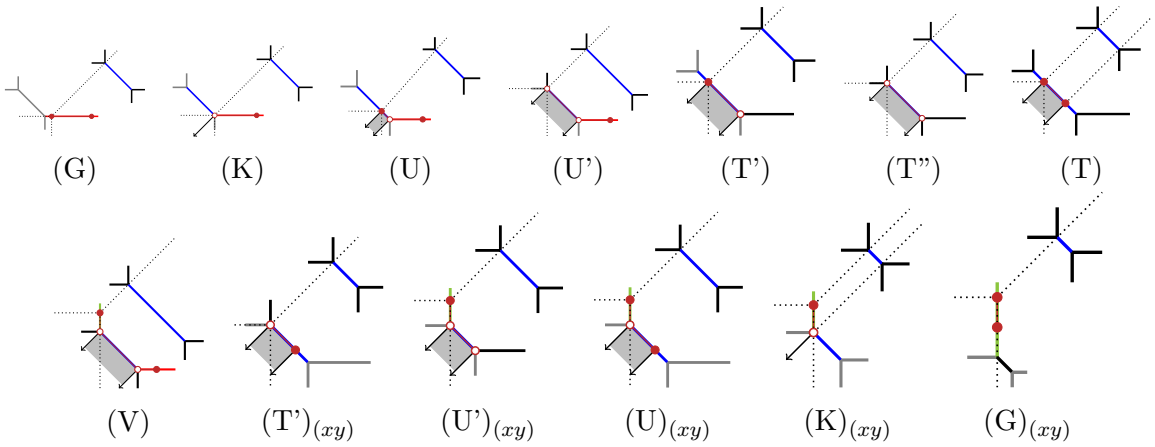

Figure 10: Deformation of bitangent shapes (G), (K), (U), (U'), (T"), (T), (V), (T'), (U')$_{(x\,y)}$, (U)$_{(x\,y)}$, (K)$_{(x\,y)}$, (G)$_{(x\,y)}$.

We see that B cannot deform into any other shapes by considering Figure 10. Rays with direction $e_1 + e_2$ passing through the vertices of $E^\vee$ cannot intersect the upper vertex of $(\overline{p_{01}p_{11}})^\vee$ or the right vertex of $(\overline{p_{10}p_{11}})^\vee$. Thus, B cannot deform further. □

Similar reasoning leads us to complete the classification in Theorem 2. Orbit representatives of the dual complexes describing the deformation classes are illustrated in Figure 11.

Proof of Theorem 2. The general idea behind the proof is as follows: We look at the classification of dual bitangent motifs summarized in Figure 4. We identify common subcomplexes in the dual bitangent motifs and check whether deformations between corresponding bitangent shapes are possible. Lemma 7 describes deformation classes with constant shapes, and Lemmas 8 and 9 cover deformation classes (E J F) and (G K U U' T T' T" V)+$(x\,y)$. The remaining cases are summarized in the following table. Figures of the deformation classes are provided in Appendix A. For details see [9].

(B H' H)	
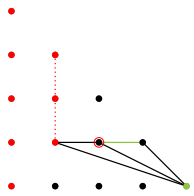	First tangency: Non-transversal intersection on $(\overline{p_{11}p_{12}})^\vee$ or $(\overline{p_{12}p_{13}})^\vee$. Second tangency: Depending on the edge lengths, vertex of the bitangent lying on the edge $(\overline{p_{21}p_{31}})^\vee$ (B), $(\overline{p_{21}p_{40}})^\vee$ (H) or on their shared vertex (H'). No further deformations: The vertices $\Delta(p_{40}p_{21}p_{11})^\vee$ resp. $\Delta(p_{21}p_{31}p_{40})^\vee$ must have y-coordinate smaller resp. larger than $(\overline{p_{11}p_{12}})^\vee$ and $(\overline{p_{12}p_{13}})^\vee$.
(B H' H)+$(y\,z)$ = (B H' H H'$_{(yz)}$ B$_{(yz)}$)	
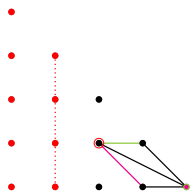	First tangency: Non-transversal intersection on $(\overline{p_{1v}p_{1,v+1}})^\vee$. Second tangency: Depending on the edge lengths, vertex of the bitangent lying on the edge $(\overline{p_{21}p_{31}})^\vee$ (B), $(\overline{p_{21}p_{40}})^\vee$ (H), $(\overline{p_{21}p_{30}})^\vee$ (B)$_{(yz)}$ or on their shared vertices (H'), (H')$_{(yz)}$ resp.. No further deformations: The lowest vertex of $(\overline{p_{21}p_{30}})^\vee$ has y-coordinate smaller than $\Delta(p_{21}p_{1v}p_{1,v+1})^\vee$.
(B M)+$(y\,z)$ = (B M B$_{(yz)}$)	
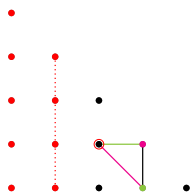	First tangency: Non-transversal intersection on $(\overline{p_{1v}p_{1,v+1}})^\vee$. Second tangency: Depending on the edge lengths, vertex of the bitangent lying on the edge $(\overline{p_{21}p_{31}})^\vee$ (B), $(\overline{p_{21}p_{30}})^\vee$ (B)$_{(yz)}$ or on the ray of direction e_1 starting at $\Delta(p_{21}p_{30}p_{31})^\vee$ (M). No further deformations: The lower vertex of $(\overline{p_{21}p_{30}})^\vee$ has always smaller y-coordinate than $\Delta(p_{1v}p_{1,v+1}p_{21})^\vee$, and the upper vertex of $(\overline{p_{21}p_{31}})^\vee$ has always larger y-coordinate than $(\overline{p_{1v}p_{1,v+1}})^\vee$.

(D L' Q)	
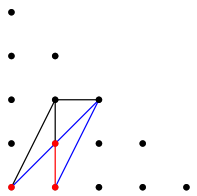	First tangency: Transversal intersection of the diagonal, vertical ray of the bitangent line with $(\overline{p_{11}p_{22}})^\vee$, $(\overline{p_{22}p_{10}})^\vee$, respectively. Second tangency: Depending on the edge lengths, the non-transversal intersection with $(\overline{p_{10}p_{11}})^\vee$ in the horizontal ray of the bitangent line (D) deforms to a transversal intersection of $(\overline{p_{00}p_{11}})^\vee$ with the diagonal ray (Q), through the shared vertex (L'). No further deformation: Due to the edge directions determined by the dual bitangent motif.
(D L' Q Q' R)	
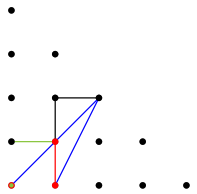	First tangency: Same as for (D L' Q). Second tangency: Depending on the edge lengths, the non-transversal intersection with $(\overline{p_{10}p_{11}})^\vee$ in the horizontal ray of the bitangent line (D) deforms through the shared vertex (L') to a transversal intersection of $(\overline{p_{00}p_{11}})^\vee$ with the diagonal ray (Q), through the shared vertex (Q') to a non-transversal intersection of $(\overline{p_{01}p_{11}})^\vee$ with the vertical ray (R). No further deformation: The upper vertex of $(\overline{p_{01}p_{11}})^\vee$ has always larger y-coordinate than any intersection of the ray of direction $-(e_1+e_2)$ starting at $\Delta(p_{22}p_{11}p_{12})^\vee$ with $(\overline{p_{01}p_{11}})^\vee$.
(D L O)	
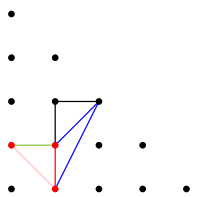	First tangency: Same as for (D L' Q). Second tangency: Depending on the edge lengths, the non-transversal intersection with $(\overline{p_{10}p_{11}})^\vee$ in the horizontal ray of the bitangent line (D) deforms through the shared vertex (L) to a non-transversal intersection of $(\overline{p_{01}p_{11}})^\vee$ with vertical ray (O). No further deformation: Same as for (D L' Q Q' R).

$\mathbf{(G\ I\ N)+(x\ y) = (G\ I\ N\ I_{(xy)}\ G_{(xy)})}$	
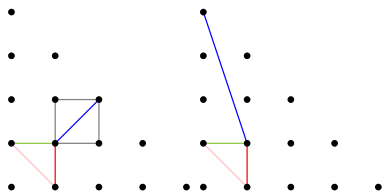	First tangency: Transversal intersection of the diagonal ray with $(\overline{p_{11}p_{22}})^\vee$, $(\overline{p_{11}p_{04}})^\vee$, respectively. Second tangency: Non-transversal intersection of the horizontal ray with $(\overline{p_{10}p_{11}})^\vee$ (G,I,N), non-transversal intersection of the diagonal ray with $(\overline{p_{10}p_{01}})^\vee$ (I,N), non-transversal intersection of the horizontal ray with $(\overline{p_{01}p_{11}})^\vee$ (N, $I_{(xy)}$,$G_{(xy)}$), depending on the edge lengths. No further deformations: Rays of direction $-(e_1 + e_2)$ starting from the two vertices of $(\overline{p_{11}p_{22}})^\vee$, $(\overline{p_{11}p_{04}})^\vee$ always intersect $(\overline{p_{01}p_{11}})^\vee$, $(\overline{p_{10}p_{11}})^\vee$ under, left of their other vertex, respectively (**not** $\Delta(p_{10}p_{01}p_{11})^\vee$).
(G K U T T')	
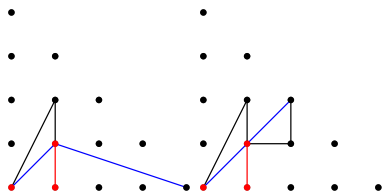	First tangency: Transversal intersection of the diagonal ray with $(\overline{p_{11}p_{40}})^\vee$, $(\overline{p_{11}p_{22}})^\vee$ respectively. Second tangency: Non-transversal intersection of the horizontal ray with $(\overline{p_{10}p_{11}})^\vee$ (G,K,U), transversal intersection of the diagonal ray with $\Delta(p_{00}p_{10}p_{11})^\vee$ (K,U,T'), transversal intersection of the diagonal ray with $(\overline{p_{00}p_{11}})^\vee$ (U,T',T), depending on the edge lengths. No further deformations: Similar to (G I N)+(x y).

(W $\mathbf{X_{(xz)}}$ $\mathbf{Y_{(xz)}}$ EE GG)	
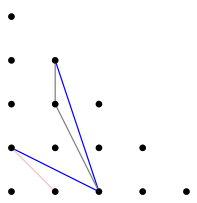	First tangency: Transversal intersection of the diagonal ray with $(\overline{p_{20}p_{13}})^\vee$. Second tangency: Transversal intersection of the horizontal ray with $(\overline{p_{01}p_{20}})^\vee$ (W). Depending on the edge lengths, additionally: Transversal intersection with $(\overline{p_{10}p_{01}})^\vee$ ($X_{(xz)}$,$Y_{(xz)}$,GG), vertex of bitangent line contained in $(\overline{p_{01}p_{20}})^\vee$ ($Y_{(xz)}$,EE,GG). No further deformations: Due to its position and slope, $(\overline{p_{20}p_{13}})^\vee$ never intersects the the bitangent class; the diagonal ray starting from $\Delta(p_{12}p_{20}p_{13})^\vee$ never meets $\Delta(p_{01}p_{20}p_{11})^\vee$; the intersection of the diagonal rays from the vertices of $(\overline{p_{20}p_{13}})^\vee$ with the horizontal rays from the vertices of $(\overline{p_{01}p_{20}})^\vee$ always lead to a 2-dimensional bounded cell.
(W…HH)+(x z) = (W X Y Z AA BB CC DD EE FF GG HH $\mathbf{X_{(xz)}}$ $\mathbf{Y_{(xz)}}$ $\mathbf{AA_{(xz)}}$ $\mathbf{CC_{(xz)}}$ $\mathbf{DD_{(xz)}}$ $\mathbf{EE_{(xz)}}$ $\mathbf{FF_{(xz)}}$ $\mathbf{GG_{(xz)}}$ $\mathbf{HH_{(xz)}}$)	
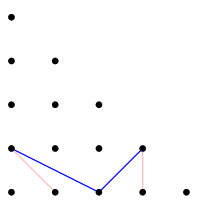	Due to (x z)-symmetry, we describe the tangency types only once. Tangency: Transversal intersection of the diagonal ray of the bitangent line with $(\overline{p_{20}p_{31}})^\vee$. Depending on the edge lengths, there are additional types: transversal intersection with $(\overline{p_{30}p_{31}})^\vee$ (X,Y,Z,AA,$AA_{(xz)}$,BB,CC,DD,FF,$GG_{(xz)}$,HH, $HH_{(xz)}$), vertex of bitangent line contained in $(\overline{p_{31}p_{20}})^\vee$ (Y,AA,BB,CC,$CC_{(xz)}$,DD,$EE_{(xz)}$, $FF_{(xz)}$,$GG_{(xz)}$,$HH_{(xz)}$). No further deformations: $(\overline{p_{20}p_{13}})^\vee$ and $(\overline{p_{01}p_{20}})^\vee$ are always in relative position such that the intersection of rays of direction $-(e_1+e_2)$ starting from the vertices of $(\overline{p_{20}p_{13}})^\vee$ with rays of direction e_1 starting from the vertices of $(\overline{p_{01}p_{20}})^\vee$ (with Γ as boundary where necessary) will always form a bounded 2-dimensional cell in the area between the two edges.

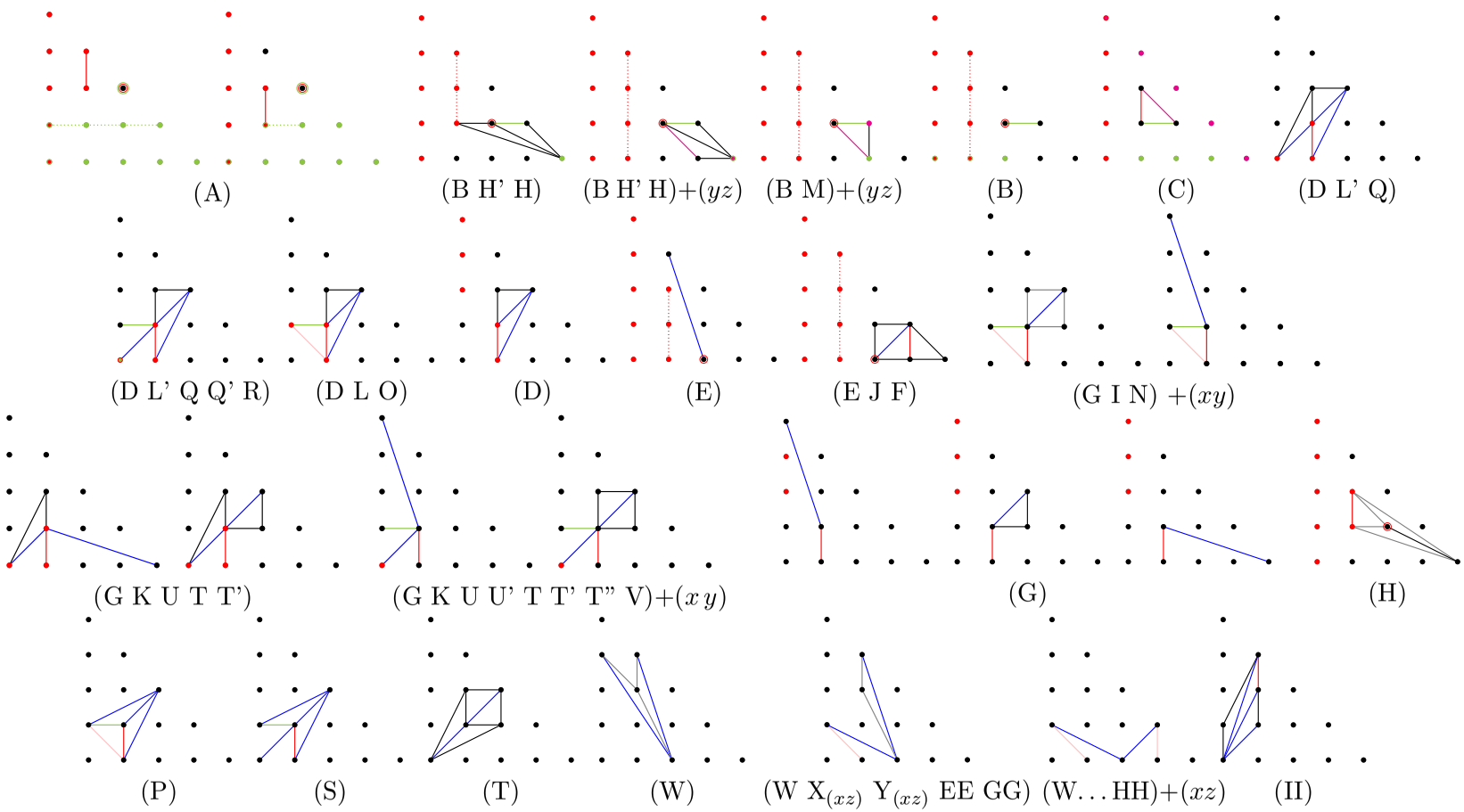

Figure 11: A list of the dual deformation motifs of all 24 deformation classes.

4 Real lifting conditions of deformation classes

In this section, we focus on the real lifting conditions determined by each shape in a deformation class. This leads to a new proof of Plücker and Zeuthen's count for tropically smooth quartics. First, we focus on the two deformation classes discussed in Lemmas 8 and 9. Then, we analyze the sign rules for the deformation class (C) which requires a special argument, as is explained in Example 12. There are six cases to treat depending on the relative order of the edge lenghts of three relevant bounded edges of Γ yielding shape (C). Sign rules for lifting the remaining deformation classes are provided in Theorem 14. Table 5 contains a summary of our fundings.

Our starting point are the real lifting conditions determined by Cueto and Markwig [6] and reported in Table 3. With the notation s_{mn} we indicate the sign of the coefficient c_{mn} of the monomial corresponding to the lattice point p_{mn}. In the proofs, we will consider five parameters i, j, k, u and v. The edge $\overline{p_{u1}p_{u+1,1}}$ is the green edge in a dual bitangent motif. The parameter j specifies the point p_{j0} forming a triangle with the green edge. The edge $\overline{p_{1v}p_{1,v+1}}$ is the red edge in a dual bitangent motif. The parameter i specifies the point p_{0i} forming a triangle with the red edge. Finally, k parametrizes a blue edge $\overline{p_{11}p_{k,4-k}}$.

Shape	Lifting conditions
(A)	$(-s_{1v}s_{1,v+1})^i s_{0i}s_{22} > 0$ and $(-s_{u1}s_{u+1,1})^j s_{j0}s_{22} > 0$
(B)	$(-s_{1v}s_{1,v+1})^{i+1} s_{0i}s_{21} > 0$ and $(-s_{21})^{j+1} s_{31}^j s_{1v}s_{1,v+1}s_{j0} > 0$
(C)	$(-s_{11})^{i+j} s_{12}^i s_{21}^j s_{0i}s_{j0} > 0$ and $(-s_{21})^{k+j} s_{12}^k s_{11}^j s_{k,4-k}s_{j0} > 0$
(H),(H')	$(-s_{1v}s_{1,v+1})^{i+1} s_{0i}s_{21} > 0$ and $-s_{21}s_{1v}s_{1,v+1}s_{40} > 0$
(M)	$(-s_{1v}s_{1,v+1})^{i+1} s_{0i}s_{21} > 0$ and $s_{31}s_{1v}s_{1,v+1}s_{30} > 0$
(D)	$(-s_{10}s_{11})^i s_{0i}s_{22} > 0$
(E),(F),(J)	$(-s_{1v}s_{1,v+1})^{i+1} s_{0i}s_{20} > 0$
(G)	$(-s_{10}s_{11})^i s_{0i}s_{k,4-k} > 0$
(I),(N)	$-s_{10}s_{11}s_{01}s_{k,4-k} > 0$
(K),(T),(T'),(T"), (U),(U'),(V)	$s_{00}s_{k,4-k} > 0$
(L),(O),(P)	$-s_{10}s_{11}s_{01}s_{22} > 0$
(L'),(Q),(Q'), (R),(S)	$s_{00}s_{22} > 0$
rest	no conditions

Table 3: The real lifting conditions of the bitangent shapes in their identity positions as determined in [6, Table 11].

Lemma 10. *Let Γ be a smooth tropical plane quartic with dual triangulation $\mathcal{T}$ and a bitangent shape B in the deformation class (E J F). For every $c \in \Sigma(\mathcal{T})$ the real lifting conditions of B_c in Γ_c are independent of the shape of the bitangent class.*

Proof. From the proof of Lemma 8 we know that a bitangent class in the deformation class (E J F) can deform into any of the three shapes, all in the same position with respect

to the action of S_3. As the triangulation $\mathcal{T}$ is fixed, the values that have to be substituted for v and i in the formula from Table 3 do not change for the three shapes. □

Lemma 11. *Let Γ be a smooth tropical plane quartic curve with dual triangulation $\mathcal{T}$ and a bitangent shape B in a deformation class (G K U U' T T' T" V)+$(x\,y)$. For every $c \in \Sigma(\mathcal{T})$ the real lifting conditions of B_c in Γ_c are independent of the shape of the bitangent class.*

Proof. Figure 9 shows the two dual deformation motifs of the deformation class. The lifting conditions of shape (G) and shapes (K), (U), (U'), (T), (T'), (T"), (V) in identity position differ by the factor $(-s_{10}s_{11})^i$. Since the vertex relevant to the value of i is p_{00}, the value of i is 0, so the two conditions coincide. This value does not change under the $(x\,y)$ permutation. The sign $s_{k,4-k}$ is uniquely determined by the dual motif, so again it stays the same for all shapes. Thus, we can conclude for both dual deformation motifs in Figure 9 that the real lifting conditions are independent of the shapes. □

We now focus on the special case of deformation class (C). In [6], the lifting conditions for the bitangent class (C) are computed for generic tropical quartics satisfying the following condition: If Γ contains a vertex v adjacent to three bounded edges with directions $-e_1$, $-e_2$ and e_1+e_2, then there exists a unique shortest edge. The vertex of a tropical bitangent of shape (C) coincides with v. Cueto and Marking chose the edge with direction $-e_2$ as shortest edge. We denote with λ_1, λ_2 and λ_3 the lattice lengths of the edges adjacent to the vertex v with direction $-e_2$, $-e_1$ and e_1+e_2, respectively. When $\lambda_1 < \lambda_2 \leqslant \lambda_3$, we call this the *identity case* of the genericity condition.

Any generic tropical quartic having a bitangent class of shape (C) at a vertex v, but with different edge lengths, can be brought into this position by applying an action of S_3. This changes the dual subdivision accordingly and, as consequence, also the formula for the real lifting conditions of (C). We illustrate this in Example 12.

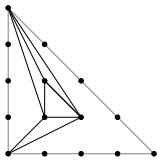

Figure 12: There are 8 unimodular triangulations refining this subdivision. Any tropical quartic curve with dual triangulation one of these 8 refinements does not satisfy the genericity condition.

For some tropical quartic curves with bitangent class (C), the genericity condition of a unique shortest edge adjacent to v can never be satisfied. This happens when the dual triangulation only allows a pair of shortest edges adjacent to v. Up to S_3-action, these triangulations are unimodular refinements of the partial subdivision in Figure 12.

Example 12. We consider the two smooth tropical quartic curves dual to the triangulation $\mathcal{T}$ shown in Figure 13. These quartic curves have a bitangent class of shape (C). For the

tropical curve in Figure 13b, the lengths $\lambda_1, \lambda_2, \lambda_3$ satisfy the identity case of the genericity condition: $\lambda_1 < \lambda_2 \leqslant \lambda_3$. We substitute $i = 2, j = 1, k = 2$ in the real lifting condition for (C) in Table 3 obtaining

$$-s_{11}s_{21}s_{02}s_{10} > 0 \text{ and } -s_{21}s_{11}s_{22}s_{10} > 0. \tag{2}$$

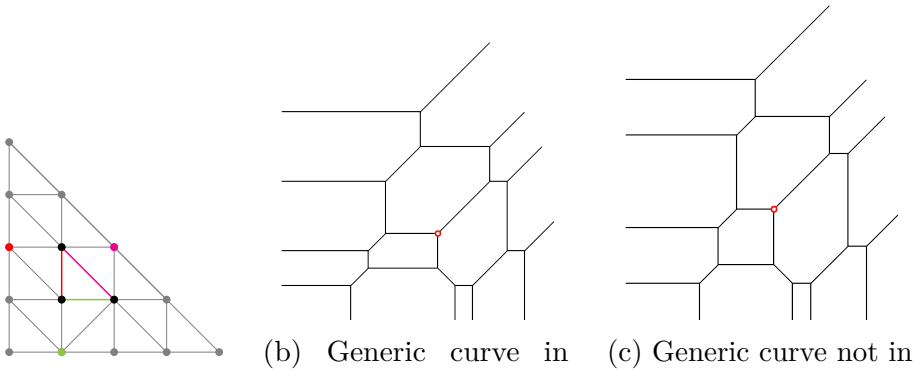

(a) Triangulation $\mathcal{T}$

(b) Generic curve in identity position.

(c) Generic curve not in identity position.

Figure 13: Smooth tropical quartic with bitangent class of shape (C). We have $i = 2$, $j = 1$, and $k = 2$.

By choosing a different weight vector in $\Sigma(\mathcal{T})$, we can deform the edge lengths such that $\lambda_2 < \lambda_1 \leqslant \lambda_3$. An example of this is shown in Figure 13c. In this case, we are no longer in the identity case, so in order to apply the lifting formula, we need to apply the action of $(x\,y)$ to switch the lengths λ_1 and λ_2, inducing also an action on the triangulation $\mathcal{T}$. The image of the curve and of $\mathcal{T}$ under $(x\,y)$ is depicted in Figure 14. Now, we have to substitute $i = 1, j = 2, k = 2$ in the lifting conditions for shape (C) obtaining

$$-s_{11}s_{12}s_{01}s_{20} > 0 \text{ and } s_{22}s_{20} > 0.$$

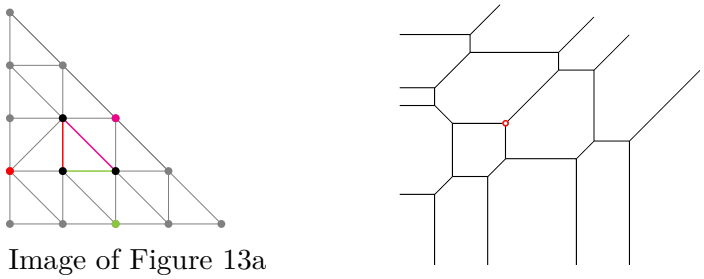

(a) Image of Figure 13a under $(x\,y)$.

(b) Image of Figure 13c under $(x\,y)$.

Figure 14: The $(x\,y)$-transformation of the tropical curve in Figure 13c and its dual triangulation. We have $i = 1$, $j = 2$, and $k = 2$.

We then deduce the lifting conditions for the original quartic with $\lambda_2 < \lambda_1 \leqslant \lambda_3$ by applying $(x\,y)^{-1} = (x\,y)$:

$$-s_{11}s_{21}s_{10}s_{02} > 0 \text{ and } s_{22}s_{02} > 0. \tag{3}$$

The second inequalities in (2) and (3) are different. However, we observe that the first inequality $-s_{11}s_{21}s_{10}s_{02} > 0$ is true if and only if $s_{02} = -s_{11}s_{21}s_{10}$. Substituting this equation into the second inequality, we see that the real lifting conditions are equivalent.

Proposition 13. *Let Γ be a smooth tropical plane quartic curve with dual triangulation $\mathcal{T}$ and a bitangent class B of shape (C). For every generic $c \in \Sigma(\mathcal{T})$, the real lifting conditions of B_c in Γ_c are equivalent.*

Proof. We fix the following notation, see also Figure 15: i is the y-coordinate of the vertex p_{0i}, which forms a triangle with the (red) edge $\overline{p_{11}p_{12}}$, j is the x-coordinate of the vertex p_{j0}, which forms a triangle with the (green) edge $\overline{p_{11}p_{21}}$ and k is the x-coordinate of the vertex $p_{k,4-k}$, which forms a triangle with the (pink) edge $\overline{p_{12}p_{21}}$.

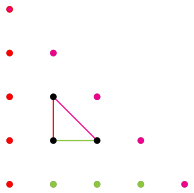

Figure 15: The dual deformation motif to shape (C) in identity position. The choices of the green, red, pink lattice points determine the values of j, i, k, respectively.

We compute the real lifting conditions of shape (C) for a bitangent class not in identity position. Suppose that Γ_c has a unique shortest edge among λ_1, λ_2, λ_3. Then, there exists $\sigma \in S_3$ such that for $\sigma(\Gamma)$ the lattice lengths of the edges adjacent to $\sigma(B)$ satisfy $\lambda_1 < \lambda_2 \leqslant \lambda_3$. This corresponds to $\sigma(B)$ being in identity position. We can then determine the real lifting condition for $\sigma(B)$ using Table 3 and the parameters from $\sigma(\mathcal{T})$. In order to do this, we first need to look at the images of the three lattice points p_{0i}, p_{j0} and $p_{k,4-k}$ under σ. Their images will lie in the boundary of $4\Delta_2$: $\sigma(p_{0i}), \sigma(p_{j0}), \sigma(p_{k,4-k}) \in \{p_{0\tilde{i}}, p_{\tilde{j}0}, p_{\tilde{k},4-\tilde{k}}\}$. Secondly, we substitute the values of the tilde indices into the lifting conditions, and then apply σ^{-1} to obtain the real lifting conditions of $B = \sigma^{-1}(\sigma(B))$ in $\Gamma = \sigma^{-1}(\sigma(\Gamma))$. Finally, we have to compare the lifting conditions of the bitangent class B of shape (C) in Γ with the ones of B_c of shape (C) in Γ_c where $c \in \Sigma(\mathcal{T})$ such that the dual deformation motif of (Γ_c,B_c) is in identity position and Γ_c satisfies $\lambda_1 < \lambda_2 \leqslant \lambda_3$.

Inequalities	Shape	Sign Rules
$\lambda_1 < \lambda_2 \leqslant \lambda_3$	(C)	$(-s_{11})^{i+j}s^i_{12}s^j_{21}s_{0i}s_{j0} > 0$ $(-s_{21})^{k+j}s^k_{12}s^j_{11}s_{k,4-k}s_{j0} > 0$
$\lambda_2 < \lambda_1 \leqslant \lambda_3$	$(\mathrm{C})_{(xy)}$	$(-s_{11})^{i+j}s^i_{12}s^j_{21}s_{0i}s_{j0} > 0$ $(-s_{12})^{k+i}s^k_{21}s^i_{11}s_{k,4-k}s_{0i} > 0$
$\lambda_3 < \lambda_2 \leqslant \lambda_1$	$(\mathrm{C})_{(xz)}$	$(-s_{21})^{k+j}s^k_{12}s^j_{11}s_{k,k-4}s_{j0} > 0$ $(-s_{11})^{i+j}s^i_{12}s^j_{21}s_{0i}s_{j0} > 0$
$\lambda_1 < \lambda_3 \leqslant \lambda_2$	$(\mathrm{C})_{(yz)}$	$(-s_{12})^{i+k}s^i_{11}s^k_{21}s_{0i}s_{k,4-k} > 0$ $(-s_{21})^{i+j}s^j_{11}s^k_{12}s_{k,4-k}s_{j0} > 0$
$\lambda_3 < \lambda_1 \leqslant \lambda_2$	$(\mathrm{C})_{(xyz)}$	$(-s_{21})^{j+k}s^j_{11}s^k_{12}s_{j0}s_{k,4-k} > 0$ $(-s_{12})^{k+i}s^i_{11}s^k_{21}s_{0i}s_{k,4-k} > 0$
$\lambda_2 < \lambda_3 \leqslant \lambda_1$	$(\mathrm{C})_{(xzy)}$	$(-s_{12})^{k+i}s^k_{21}s^i_{11}s_{k,4-k}s_{0i} > 0$ $(-s_{11})^{j+i}s^j_{21}s^i_{12}s_{j0}s_{0i} > 0$

The sign rules in the table are obtained by applying the corresponding permutation to each formula for the identity position (row 1 of the table) and replacing the values of i, j, k by the corresponding ones. The procedure should be clear from Figure 1. For example, when applying (xyz), the values of (i, j, k) should be replaced with (j, k, i).

Then, it suffices to use the same techniques as in Example 12 to confirm the sign rules for all 6 cases are equivalent. For example, to show the equivalence between cases 1 and 2, it is enough to check that the first inequalities in both cases agree, whereas replacing s_{j0} by $(-s_{11})^{i+j} s_{12}^i s_{21}^j s_{0i}$ (which follows from the first inequality) in the second inequality for case 1 yields the remaining inequality in case 2. The equivalence between case 1 and the remaining cases follows by similar reasoning since they always share a common inequality. □

Theorem 14. *Let Γ be a generic tropical smooth quartic curve with dual triangulation $\mathcal{T}$, and let B be a tropical bitangent class. For every $c \in \Sigma(\mathcal{T})$, the real lifting conditions of B_c in Γ_c are independent on the shape of the bitangent class. In other words: real lifting conditions of tropical bitangent classes only depend on the dual subdivision $\mathcal{T}$ of Γ.*

Proof. We prove this by going through all deformation classes not considered in Lemma 10 and 11 and Proposition 13, and by comparing the lifting conditions of the different shapes. The shapes in the deformation classes (W $X_{(xz)}$ $Y_{(xz)}$ EE GG) and (W...HH) have no real lifting conditions, so the statement holds. The remaining deformation classes are summarized below. For the lifting conditions of the shapes we refer to Table 3.

Deformation class	parameters
(B H' H), (B H' H)+(*y z*)	The dual bitangent motif of (B) yields $j = 4$. Substituting it gives the same real lifting conditions for (B), (H') and (H). The lifting conditions for (H) and $(H)_{(y\,z)}$ are the same, so the statement follows by symmetry.
(B M)+(*y z*)	The dual bitangent motif of (B) yields $j = 3$. Substituting it gives the same real lifting conditions for (B) and (M). The real lifting conditions for (M) and $(M)_{(y\,z)}$ are the same.
(D L' Q), (D L' Q Q' R)	The dual bitangent motif of shape (D) yields $i = 0$, so the real lifting conditions for all shapes in the two deformation classes coincide.
(D L O)	The dual bitangent motif of shape (D) yields $i = 1$, so the real lifting conditions for all shapes in this deformation class coincide.
(G I N)+(*x y*)	The dual bitangent motif of shape (G) yields $i = 1$, so the real lifting conditions of (G), (I) and (N) coincide. Also, (N) and $(N)_{(x\,y)}$ have the same real lifting conditions.

Deformation class	parameters
(G K U T T')	The dual bitangent motif of shape (G) yields $i = 0$, so the real lifting conditions for all shapes in this deformation class coincide.

□

Remark 15. Markwig, Payne and Shaw characterize the lifting conditions of bitangent shapes over more general fields [16]. An analogous investigation to the proof of Theorem 14 shows that the lifting conditions again stay constant in every deformation class. Therefore, deformation classes are relevant for the lifting behavior of tropical bitangents over other fields, not only over real closed fields.

Table 5 summarizes the real lifting conditions for the deformation classes described in Lemmas 10, 11, Proposition 13 and Theorem 14.

Deformation class	Lifting conditions
(A)	$(-s_{1v}s_{1,v+1})^i s_{0i}s_{22} > 0$ and $(-s_{u1}s_{u+1,1})^j s_{j0}s_{22} > 0$
(B H' H), (B H' H)+(yz), (H)	$(-s_{1v}s_{1,v+1})^{i+1} s_{0i}s_{21} > 0$ and $-s_{21}s_{1v}s_{1,v+1}s_{40} > 0$
(B M)+(yz)	$(-s_{1v}s_{1,v+1})^{i+1} s_{0i}s_{21} > 0$ and $s_{31}s_{1v}s_{1,v+1}s_{30} > 0$
(B)	$(-s_{1v}s_{1,v+1})^{i+1} s_{0i}s_{21} > 0$ and $(-s_{21})^{j+1} s_{31}^j s_{1v}s_{1,v+1}s_{j0} > 0$ with $j \in \{0,1,2\}$
(C)	$(-s_{11})^{i+j} s_{12}^i s_{21}^j s_{0i}s_{j0} > 0$ and $(-s_{21})^{k+j} s_{12}^k s_{11}^j s_{k,4-k}s_{j0} > 0$
(D)	$(-s_{10}s_{11})^i s_{0i}s_{22} > 0$ with $i \in \{2,3,4\}$
(D L O), (P)	$-s_{10}s_{11}s_{01}s_{22} > 0$
(D L' Q), (D L' Q Q' R), (S), (T)	$s_{00}s_{22} > 0$
(E), (E J F)	$(-s_{1v}s_{1,v+1})^{i+1} s_{0i}s_{20} > 0$
(G)	$(-s_{10}s_{11})^i s_{0i}s_{k,4-k} > 0$ with $i \in \{2,3,4\}$
(G I N)+(xy)	$-s_{10}s_{11}s_{01}s_{k,4-k} > 0$
(G K U U' T T'), (G K U U' T- - T' T" V)+(xy)	$s_{00}s_{k,4-k} > 0$
rest	no conditions

Table 5: Real lifting conditions of the deformation classes in their positions as in Figure 11.

We are now ready to give a proof of our main result.

Proof of Theorem 1. Let Γ be a generic tropicalization of a tropically smooth quartic curve $V(f)$ defined over $\mathbb{K}_\mathbb{R}$ and $\mathcal{T}$ its dual triangulation. By Theorem 14, the real lifting conditions of the 7 bitangent classes of Γ only depend on their 7 deformation classes. Furthermore, the deformation classes are uniquely determined by their dual deformation motifs in the triangulation $\mathcal{T}$, as pointed out in Remark 6. Therefore, the real lifting

conditions for the tropical bitangent classes of Γ only depend on the triangulation $\mathcal{T}$.

In order to prove the statement, we need to enumerate the dual deformation motifs of the deformation classes in the 1278 unimodular regular triangulations of $4\Delta_2$ modulo S_3-symmetry as computed in [4]. Of these S_3-representatives exactly eight do not satisfy the genericity constraint that a vertex of the curve with adjacent edges of directions $-e_1$, $-e_2$, e_1+e_2 needs to have a unique shortest adjacent edge, see Figure 12. For these eight cones we did run the same computations as for the generic cones, but we could not compute the lifting behavior of the bitangent class of shape (C) since this is not yet understood. However, since the numbers of real bitangents are already known classically, our computations might help to understand these special cases.

We implemented the search for the dual deformation motifs of the deformation classes in `polymake` [8]. For each deformation class, we considered the real lifting conditions determined in Theorem 14 and summarized in Table 5, and we evaluated them for all possible 2^{15} sign vectors. Again, we implemented this in `polymake` obtaining that each sign vector satisfies the lifting conditions of 1, 2, 4 or 7 deformation classes. A more detailed description of the computational procedure and codes can be found in [10].

Finally, by [6, Theorem 1.2 and Corollary 7.3], each bitangent class has either zero or exactly four lifts to totally real bitangents. Therefore, the smooth quartic curve $V(f)$ with smooth tropicalization Γ has either 4, 8, 16 or 28 totally real bitangents. □

Example 16. We consider the following regular unimodular triangulation of $4\Delta_2$:

$$\Big[[p_{00}p_{10}p_{01}],\,[p_{01}p_{11}p_{02}],\,[p_{02}p_{21}p_{12}],\,[p_{02}p_{12}p_{03}],[p_{03}p_{13}p_{04}],\,[p_{11}p_{02}p_{21}],\,[p_{10}p_{20}p_{11}],[p_{20}p_{30}p_{31}],$$
$$[p_{30}p_{40}p_{31}],\,[p_{21}p_{31}p_{22}],[p_{12}p_{22}p_{13}],[p_{10}p_{01}p_{11}],\,[p_{12}p_{03}p_{13}],\,[p_{30}p_{21}p_{31}],\,[p_{20}p_{11}p_{21}],[p_{21}p_{12}p_{22}]\Big].$$

It contains six dual deformation motifs of type (A) and one of type (G I N)+(xy).

Deformation class	Lifting conditions
(A)	$-s_{12}s_{03}s_{22}s_{13}>0$ and $-s_{30}s_{21}s_{31}s_{22}>0$
$(\mathrm{A})_{(xz)}$	$-s_{02}s_{12}s_{03}s_{13}>0$ and $s_{20}s_{02}>0$
$(\mathrm{A})_{(xz)}$	$-s_{02}s_{12}s_{03}s_{13}>0$ and $-s_{10}s_{01}s_{11}s_{20}>0$
$(\mathrm{A})_{(xyz)}$	$-s_{10}s_{01}s_{11}s_{20}>0$ and $s_{02}s_{22}>0$
$(\mathrm{A})_{(xzy)}$	$-s_{20}s_{30}s_{21}s_{31}>0$ and $-s_{10}s_{01}s_{20}s_{11}>0$
$(\mathrm{A})_{(xz)}$	$s_{02}s_{22}>0$ and $s_{20}s_{02}>0$
$\big((\mathrm{G\ I\ N})+(xy)\big)_{(xz)}$	$-s_{20}s_{30}s_{21}s_{31}>0$

Of the 15 coefficients of the lifted algebraic curve, the maximal number of 12 is involved in the sign conditions. We fix all signs s_{ij} positive except for s_{10}, s_{21} and s_{03}. When varying these three signs, different lifting conditions will be satisfied, and consequently, the lifted real algebraic quartic curves will have different numbers of bitangent lines as summarized in the table below. The topological type of the curves near the tropical limit is also determined by the signs and can visualized via patchworking in `polymake` [12].

Negative signs	Plücker numbers	Topological type
None	4	1 oval
s_{10}	8	2 ovals
s_{10}, s_{21}	16	3 ovals
s_{10}, s_{21} and s_{03}	28	4 ovals

Acknowledgements

We are very grateful to Hannah Markwig, Angelica Cueto and Michael Joswig for valuable discussions on the topic and for their comments on earlier versions of this work. We want to thank the anonymous referee for the detailed report which helped us to improve this paper. We thank Hannah Markwig and Angelica Cueto for allowing us to include figures from their paper [6] and Hannah Markwig, Sam Payne and Kris Shaw for explaining us their project. The first author was funded by a PhD scholarship from the Cusanuswerk e.V.. This work is a contribution to the SFB-TRR 195 'Symbolic Tools in Mathematics and their Application' of the German Research Foundation (DFG).

References

[1] Daniele Alessandrini. Logarithmic limit sets of real semi-algebraic sets. *Adv. Geom.*, 13(1):155–190, 2013.

[2] Matthew Baker, Yoav Len, Ralph Morrison, Nathan Pflueger, and Qingchun Ren. Bitangents of tropical plane quartic curves. *Math. Z.*, 282(3-4):1017–1031, 2016.

[3] Saugata Basu, Richard Pollack, and Marie-Françoise Roy. *Algorithms in Real algebraic geometry*, volume 36. Springer Berlin Heidelberg, 2006.

[4] Sarah Brodsky, Michael Joswig, Ralph Morrison, and Bernd Sturmfels. Moduli of tropical plane curves. *Res. Math. Sci.*, 2:Art. 4, 31, 2015.

[5] Melody Chan and Pakawut Jiradilok. Theta characteristics of tropical K_4-curves. In *Combinatorial algebraic geometry*, volume 80 of *Fields Inst. Commun.*, pages 65–86. Fields Inst. Res. Math. Sci., Toronto, ON, 2017.

[6] Maria Angelica Cueto and Hannah Markwig. Combinatorics and real lifts of bitangents to tropical quartic curves. *Discrete Comput. Geom.*, 69:597–658, 2023.

[7] Jesús A. De Loera, Jörg Rambau, and Francisco Santos. *Triangulations*, volume 25 of *Algorithms and Computation in Mathematics*. Springer-Verlag, Berlin, 2010. Structures for algorithms and applications.

[8] Ewgenij Gawrilow and Michael Joswig. `polymake`: a framework for analyzing convex polytopes. In *Polytopes—combinatorics and computation (Oberwolfach, 1997)*, volume 29 of *DMV Sem.*, pages 43–73. Birkhäuser, Basel, 2000.

[9] Alheydis Geiger. Tropical geometric counting problems. http://hdl.handle.net/10900/132336, 2022. PhD Thesis.

[10] Alheydis Geiger and Marta Panizzut. Computing tropical bitangents of smooth quartics in `polymake`. *J. Symbolic Comput.*, 120, 2024.

[11] Michael Joswig, Marta Panizzut, and Bernd Sturmfels. The Schläfli fan. *Discrete Comput. Geom.*, 64(2):355–381, 2020.

[12] Michael Joswig and Paul Vater. Real tropical hyperfaces by patchworking in `polymake`. In *Mathematical software—ICMS 2020*, volume 12097 of *Lecture Notes in Comput. Sci.*, pages 202–211. Springer, Cham, [2020] ©2020.

[13] Heejong Lee and Yoav Len. Bitangents of non-smooth tropical quartics. *Port. Math.*, 75(1):67–78, 2018.

[14] Yoav Len and Hannah Markwig. Lifting tropical bitangents. *J. Symbolic Comput.*, 96:122–152, 2020.

[15] Diane Maclagan and Bernd Sturmfels. *Introduction to tropical geometry*, volume 161 of *Graduate Studies in Mathematics*. American Mathematical Society, Providence, RI, 2015.

[16] Hannah Markwig, Kris Shaw, and Sam Payne. Bitangents to plane quartics via tropical geometry: $\mathbb{A}^1$-enumeration, rationality, and avoidance loci. arXiv:2207.01305, 2022.

[17] Victor. P. Maslov. On a new superposition principle for optimization problem. *Séminaire Équations aux dérivées partielles (Polytechnique) dit aussi "Séminaire Goulaouic-Schwartz"*, 1985-1986.

[18] Marta Panizzut and Magnus Dehli Vigeland. Tropical lines on cubic surfaces. *SIAM J. Discrete Math.*, 36(1):383–410, 2022.

[19] Julius Plücker. Solution d'une question fondamentale concernant la théorie générale des courbes. *Journal für die reine und angewandte Mathematik*, 12:111–114, 1834.

[20] Julius Plücker. *Theorie der algebraischen Curven: gegründet auf eine neue Behandlungsweise der analytischen Geometrie*. Bonn: Adolph Marcus., 1839.

[21] Hieronymus Georg Zeuthen. Sur les diférentes formes des curbes planes du quatrième ordre. *Math. Ann.*, 7:408–432, 1873.

A

In this section we provide further figures to help understanding the classification statement in Section 3. We recommend considering the figures together with the table in the proof of Theorem 2.

A.1 Example of deformation class (B H' H)

Let Γ be a smooth tropical quartic curve with a bitangent class B with dual bitangent motif in identity position contained in the subcomplex in Figure 16. Note that we are choosing the red edge $\overline{p_{12}p_{13}}$ in the corresponding picture in Figure 11. A similar example can be drawn for $\overline{p_{11}p_{12}}$.

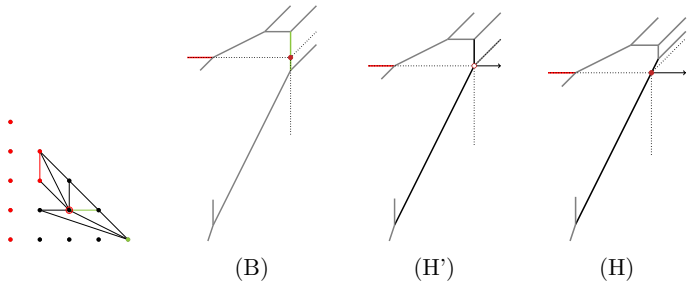

Figure 16: Example of deformation class (B H' H).

A.2 Example of deformation class (B H' H)+($y\,z$)

Let Γ be a smooth tropical quartic curve with a bitangent class B with dual bitangent motif in identity position contained in the subcomplex in Figure 17. Note that we are choosing the red edge $\overline{p_{12}p_{13}}$ in the corresponding picture in Figure 11. Similar examples can be drawn for $\overline{p_{10}p_{11}}$ and $\overline{p_{11}p_{12}}$.

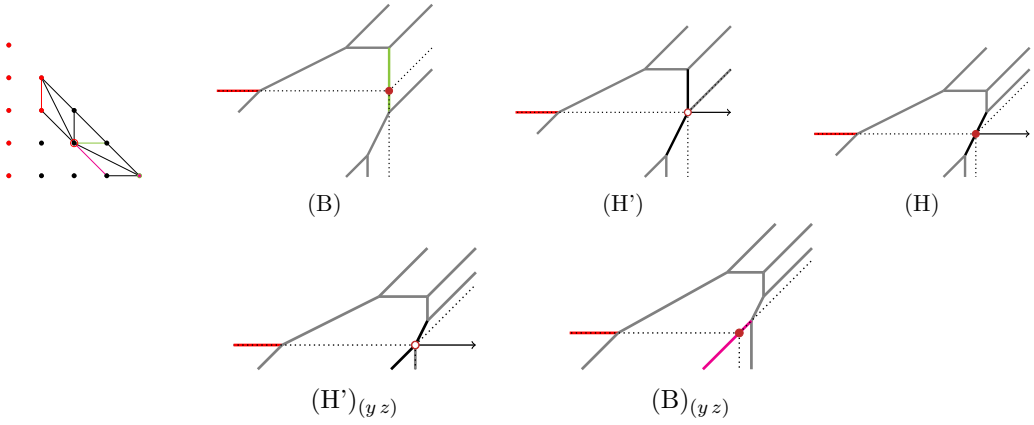

Figure 17: Example of deformation class (B H' H)+($y\,z$).

A.3 Example of deformation class (B M)+($y\,z$)

Let Γ be a smooth tropical quartic curve with a bitangent class B with dual bitangent motif in identity position contained in the subcomplex in Figure 18. Note that we are choosing the red edge $\overline{p_{12}p_{13}}$ in the corresponding picture in Figure 11. Similar examples can be drawn for $\overline{p_{10}p_{11}}$ and $\overline{p_{11}p_{12}}$.

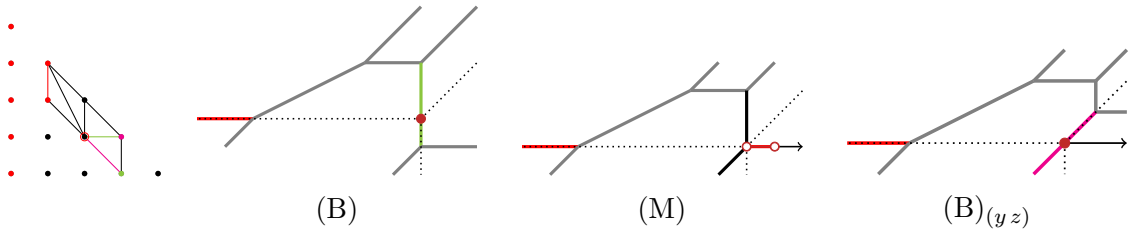

Figure 18: Example of deformation class (B M)+($y\,z$).

A.4 Example of deformation class (D L' Q)

Let Γ be a smooth tropical quartic curve with a bitangent class B with dual bitangent motif in identity position contained in the subcomplex in Figure 19.

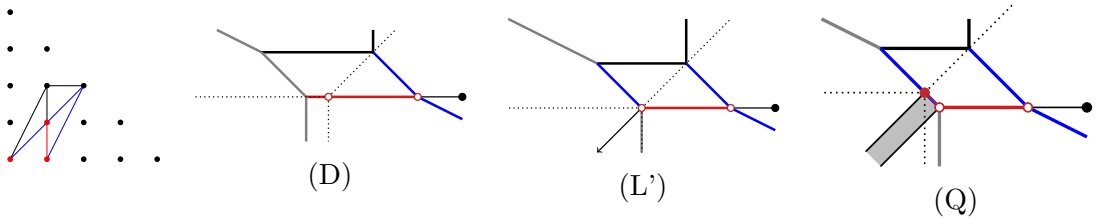

Figure 19: Example of deformation class (D L' Q).

A.5 Example of deformation class (D L' Q Q' R)

Let Γ be a smooth tropical quartic curve with a bitangent class B with dual bitangent motif in identity position contained in the subcomplex in Figure 20.

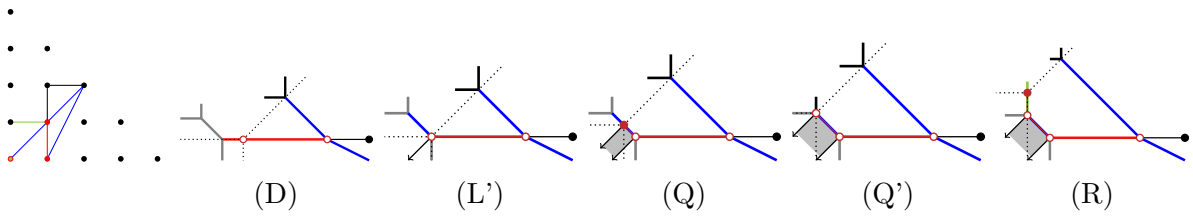

Figure 20: Example of deformation class (D L' Q Q' R).

A.6 Example of deformation class (D L O)

Let Γ be a smooth tropical quartic curve with a bitangent class B with dual bitangent motif in identity position contained in the subcomplex in Figure 21.

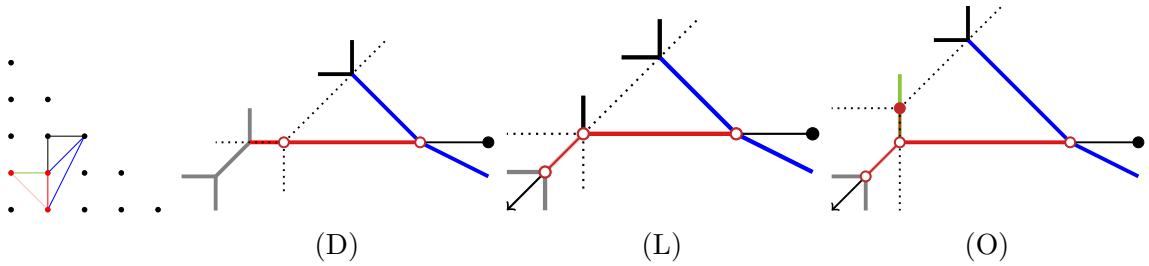

Figure 21: Example of deformation class (D L O).

A.7 Deformation class (G I N)+($x\,y$)

For this deformation class there are two different cases of how the second tangency arises. Let Γ be a smooth tropical quartic curve with a bitangent class B with dual bitangent motif in identity position contained in the subcomplex in Figure 22. This figure depicts the case where one tangency is given by the blue edge $\overline{p_{11}p_{22}}$.

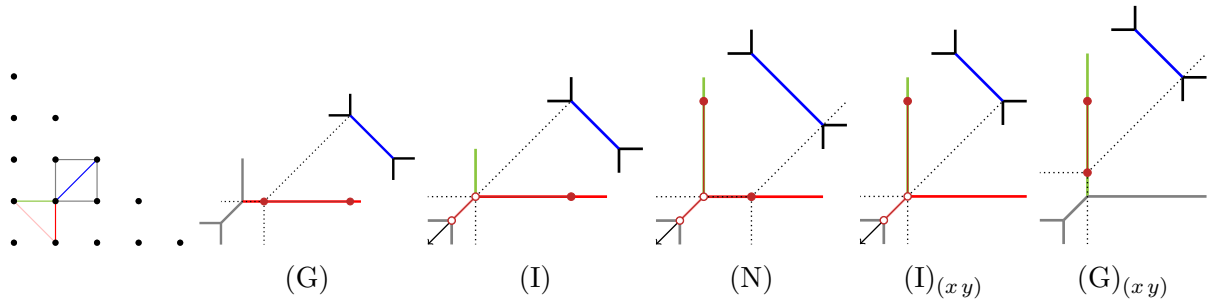

Figure 22: Example of deformation class (G I N)+($x\,y$) with one tangency given by $\overline{p_{11}p_{22}}$.

The situation is similar if we choose the other blue edge $\overline{p_{11}p_{04}}$, as illustrated in Figure 23.

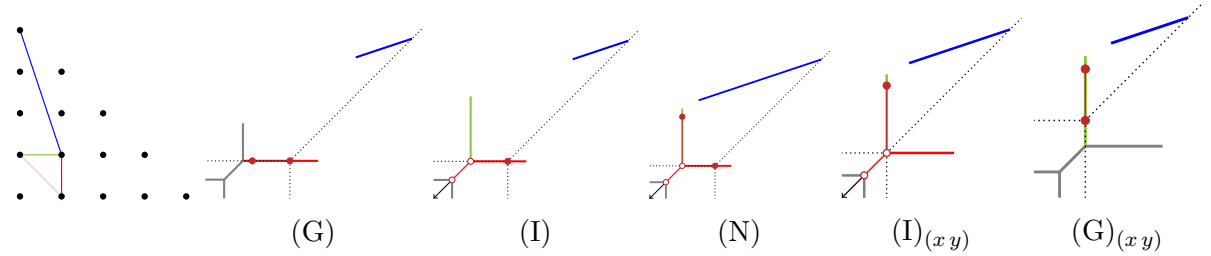

Figure 23: Example of deformation class (G I N)+($x\,y$) with one tangency given by $\overline{p_{11}p_{04}}$.

A.8 Deformation class (G K U T T')

As for deformation class (G I N)+($x\,y$) there are two different cases of how the second tangency arises. Let Γ be a smooth tropical quartic curve with a bitangent class B with dual bitangent motif in identity position contained in the subcomplex in Figure 24. This figure depicts the case where one tangency is given by the blue edge $\overline{p_{11}p_{22}}$.

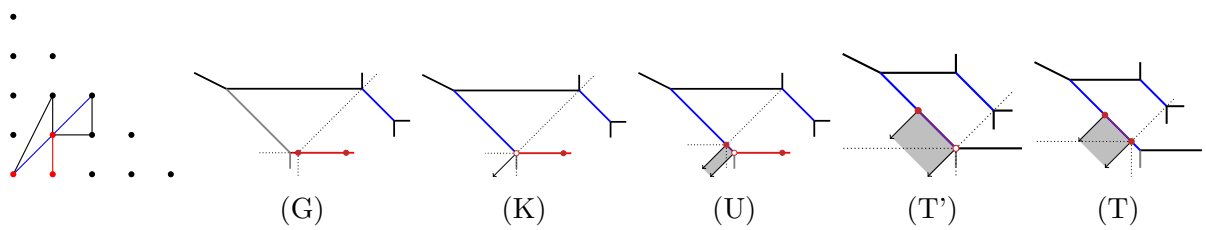

Figure 24: Example of deformation class (G K U T T') with one tangency given by $\overline{p_{11}p_{22}}$.

The situation is similar if we choose the other blue edge $\overline{p_{11}p_{40}}$, as illustrated in Figure 25.

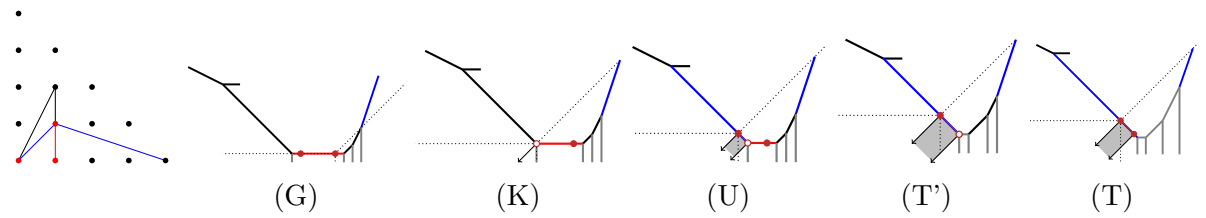

Figure 25: Example of deformation class (G K U T T') with one tangency given by $\overline{p_{11}p_{40}}$.

A.9 Deformation class (W $\mathbf{X}_{(xz)}$ $\mathbf{Y}_{(xz)}$ EE GG)

Let Γ be a smooth tropical quartic curve with a bitangent class B with dual bitangent motif in identity position contained in the subcomplex in Figure 26.

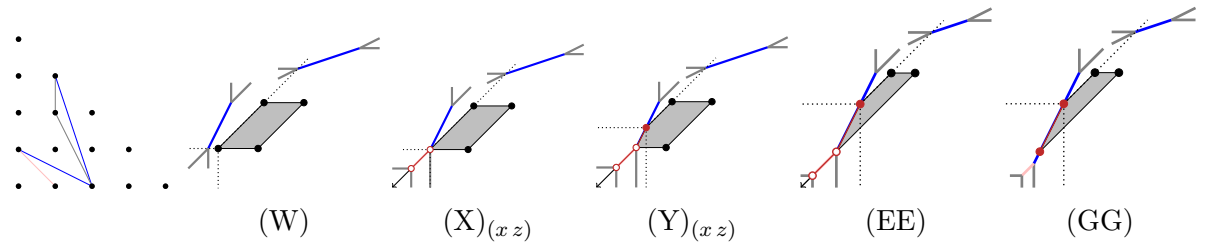

Figure 26: Example of deformation class (W $\mathrm{X}_{(xz)}$ $\mathrm{Y}_{(xz)}$ EE GG).

A.10 Deformation class (W...HH)+($x\,z$)

Let Γ be a smooth tropical quartic curve with a bitangent class B with dual bitangent motif in identity position contained in the subcomplex in Figure 27.

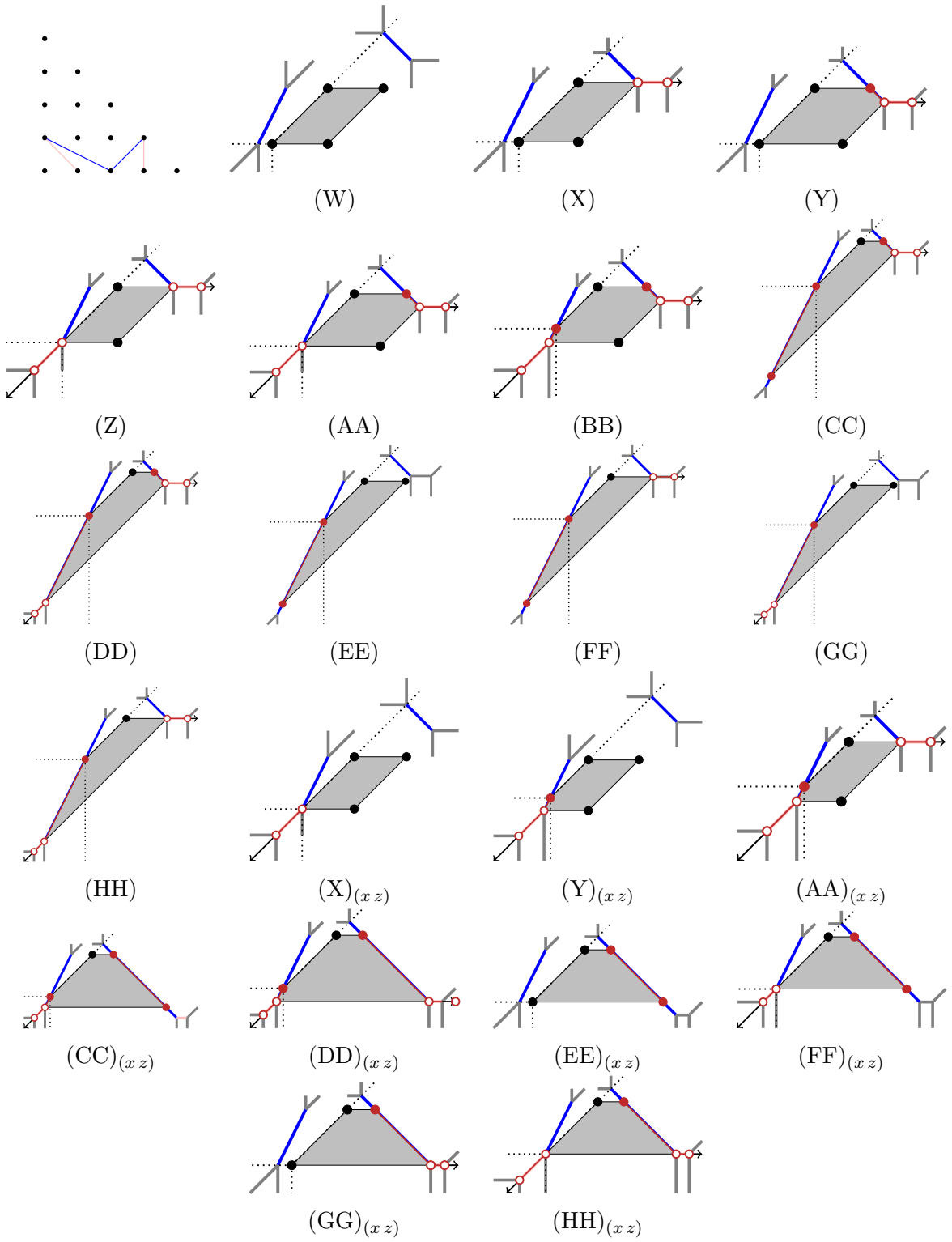

Figure 27: Example of deformation class (W X Y Z AA ... HH).